Supporting Information

Takata et al. 10.1073/pnas.0807346106

SI Text

Global maps of vegetation in 1700 and 1850 are shown in Fig. S1. The red areas indicate cultivated areas. Most of the cultivated land was originally forest, except for a few grid points (e.g., on the western edges of the cultivated area in eastern China). These areas had originally been grassland, and because vegetation height and LAI are similar for grasslands and croplands, the surface wind speed did not change at those points. The surface albedo was slightly decreased by <0.01 due to the larger LAI for croplands than for grasslands. However, the albedo decrease had no discernible effects because its area and magnitude were small. Large area was also cultivated intensively in Western Europe during 1700–1850. This land use/cover change may have an impact in the winter, but is generally insignificant in the summer.

We display the increase in surface wind speed that reached the lower troposphere by the longitude–height cross-sections of changes in the horizontal winds, in addition to the changes in 850-hPa wind vectors (Fig. 2*A*). The cross-section at 20°N shows that the westerly wind increased from 75°E to 85°E, which corresponds to the western Indian subcontinent (the IND region; Fig. S2*a*, shown by rightward vectors). The cross-section at 30°N shows that the southerly wind increased from 100°E to 120°E; this corresponds to southeastern China (SCH region; Fig. S2*b*, shown by upward vectors).

The effects of the reduction in clouds in the IND and SCH regions are clearly indicated by the increase in downward short-wave radiation (Fig. S3*a*). This corresponds with the regions where there was an increase in the net short-wave radiation absorbed at the surface (contours in Fig. 2*C*). Therefore, the increase in net short-wave radiation was induced by the increase in downward short-wave radiation, and hence the reduction in clouds, that is associated with a decrease in precipitation. In those regions, the surface soil moisture decreased, latent heat flux decreased, sensible heat flux increased, and air temperature at 2-m height increased (Fig. S3 *b–e*).

The effects of the increase in surface albedo appeared as a decrease in net short-wave radiation in ECH (Fig. 2*C*), occurring without a considerable decrease in downward short-wave radiation (Fig. S3*a*). In addition, outgoing long-wave radiation increased (Fig. S3*f*), as a result of the increase in the upward terrestrial radiation due to the surface temperature increase (Fig. S3*g*) and as a result of the decrease in downward long-wave radiation due to the moisture decrease near the surface (Fig. S3*h*). Summing those effects shows that the net radiation absorbed at the surface was decreased. A reduction in net radiation could result in a surface temperature decrease, but this effect appeared only at ≈30°N, 110–120°E, and was ≈0.5–1 °C (Fig. S3*e*). At this location, surface soil moisture was not decreased (Fig. S3*b*).

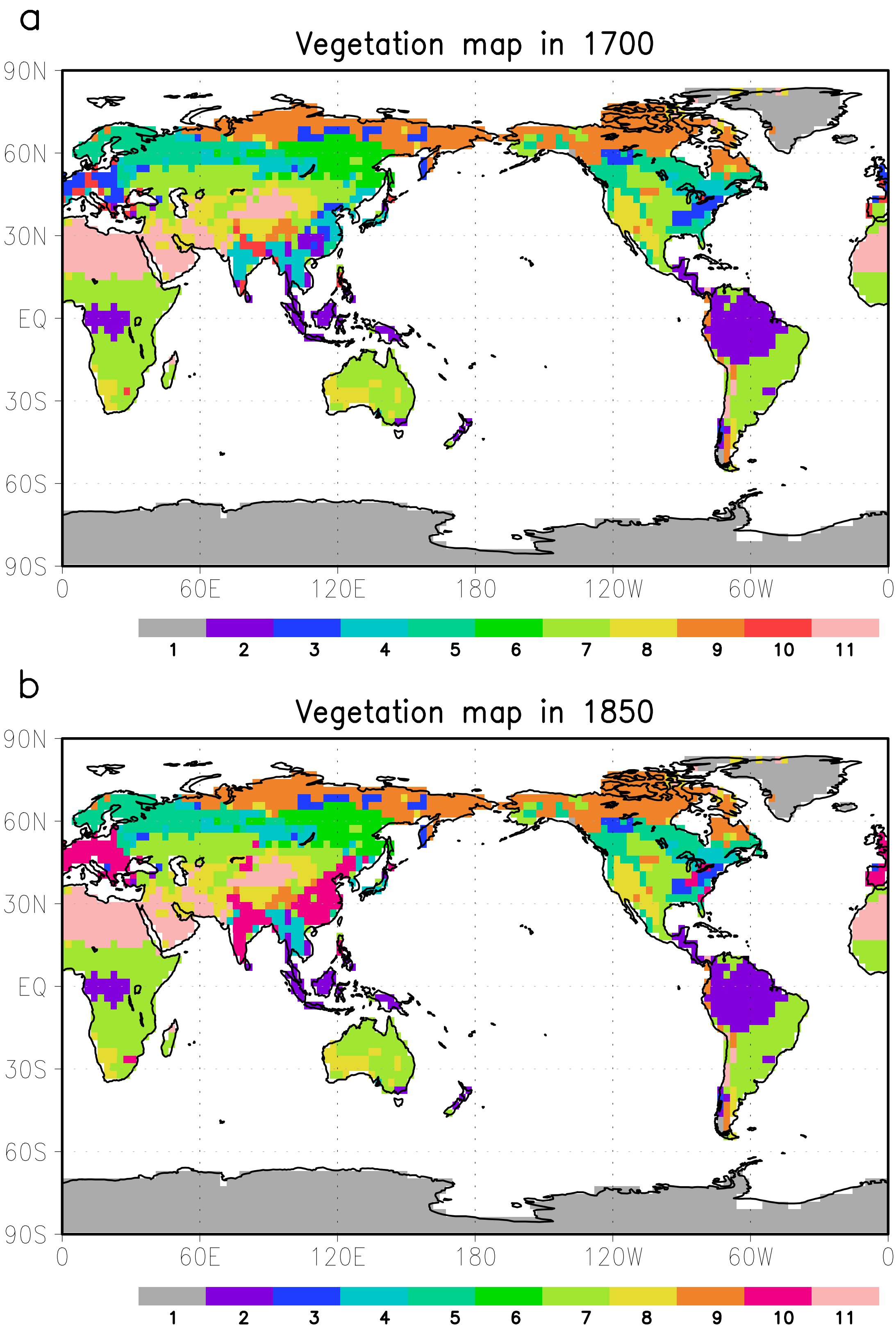

Fig. S1. Land cover distribution used in this study. (*a*) In 1700. (*b*) In 1850. Index: 1, ice; 2–6, forest; 7–9, grassland; 10, cropland; and 11, desert.

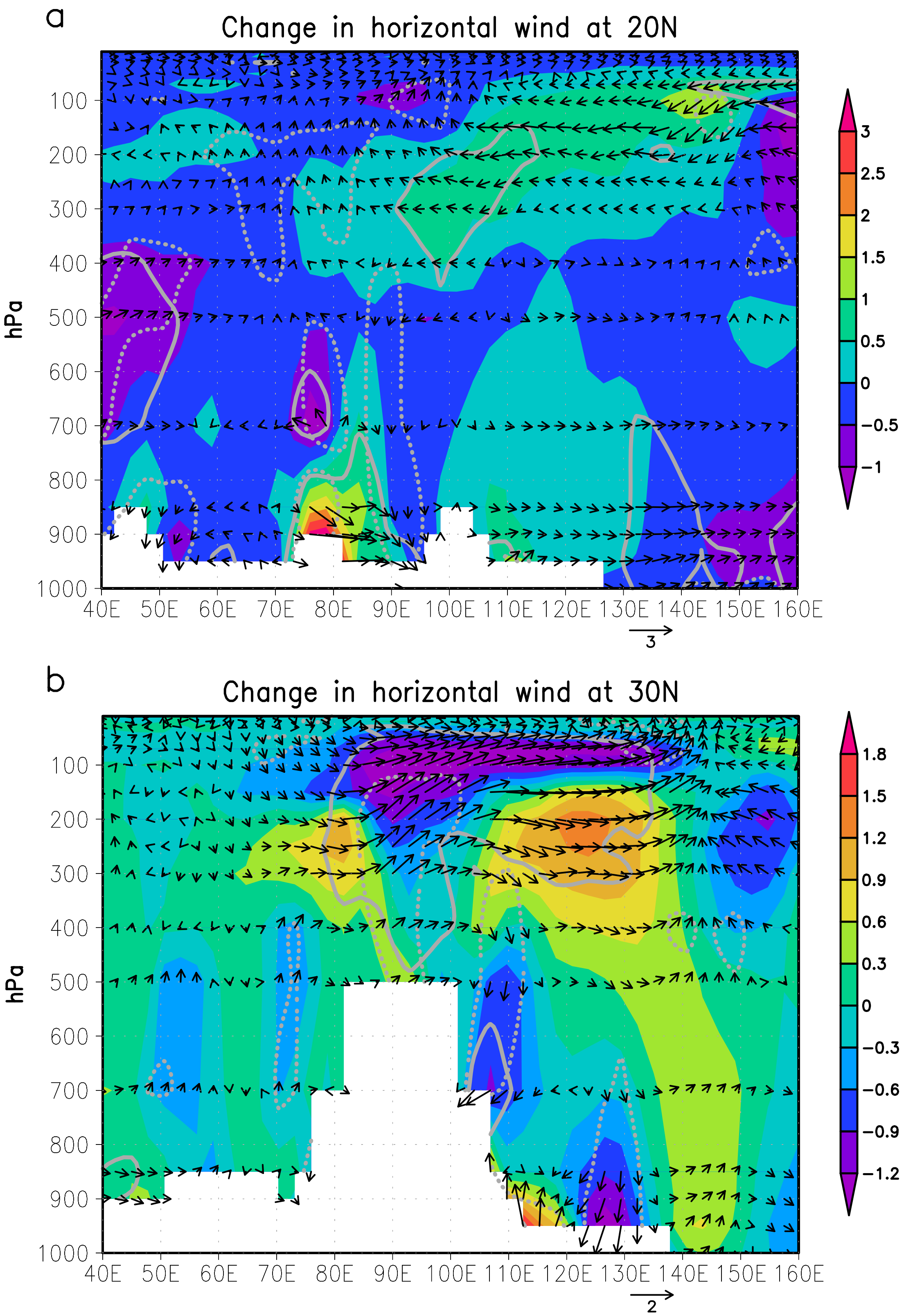

Fig. S2. Longitude–height cross-sections of June–August mean changes in horizontal wind speed (shades, in meters·s^{-1}) and horizontal wind vector (arrows, unit vector in meters·s^{-1}) between 1700 and 1850. (*a*) At 20°N. (*b*) At 30°N. The gray solid and dotted lines represent the regions in which the differences in zonal (east–west) and meridional (north–south) wind are statistically significant at the 95% confidence level.

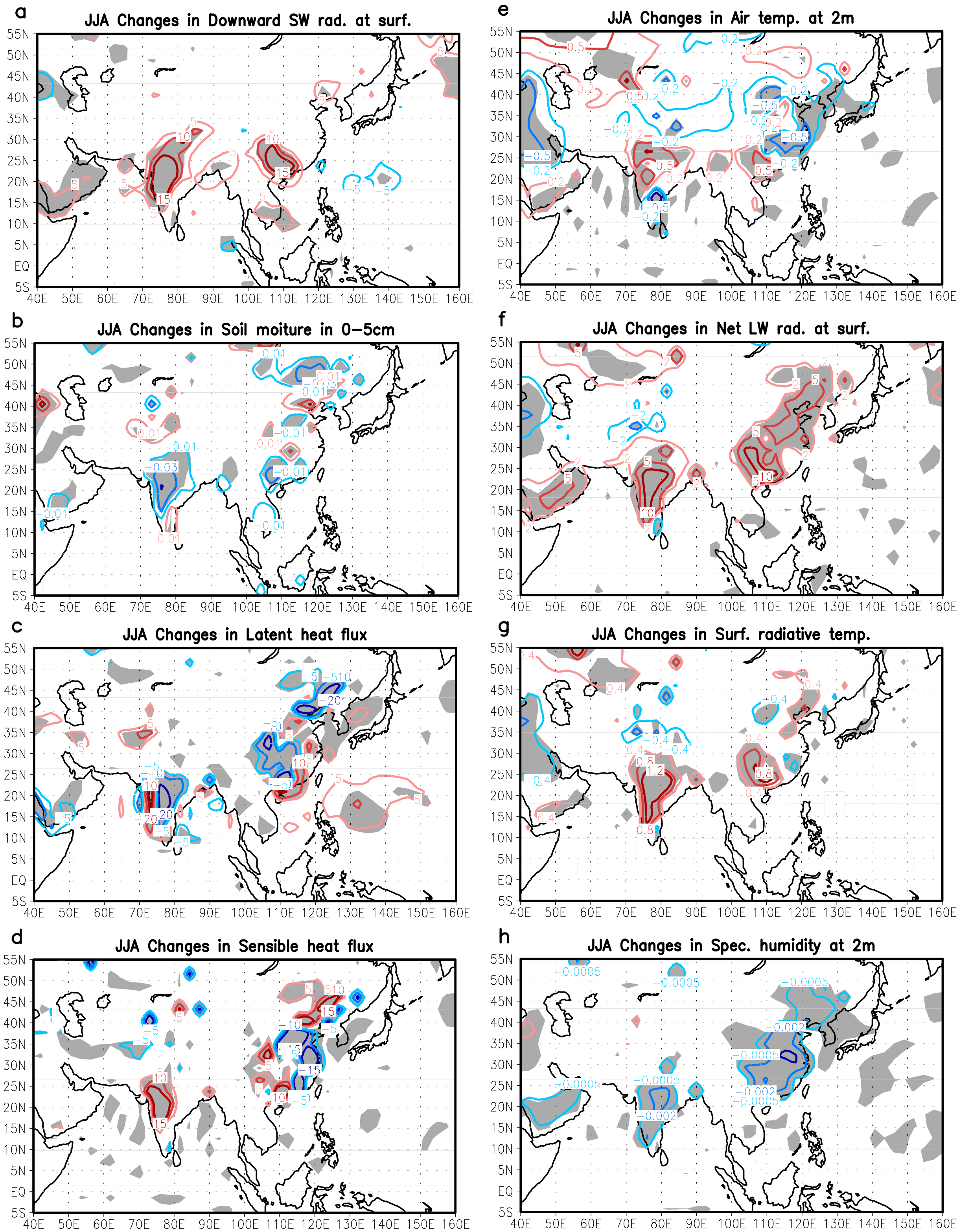

Fig. S3. June–August mean changes between 1700 and 1850. (*a*) Downward short-wave radiation in W·m^{-2}. (*b*) Volumetric soil moisture ratio in the top 0- to 5-cm layer. (*c*) Latent heat flux in W·m^{-2}. (*d*) Sensible heat flux in W·m^{-2}. (*e*) The 2-m height air temperature in K. (*f*) Net long-wave radiation (upward positive) in W·m^{-2}. (*g*) The surface radiative temperature in K. (*h*) The 2-m height-specific humidity in kg kg^{-1}. Negative values are indicated by blue contours and positive values by red contours. Shaded regions are those in which the differences are statistically significant at the 95% confidence level.

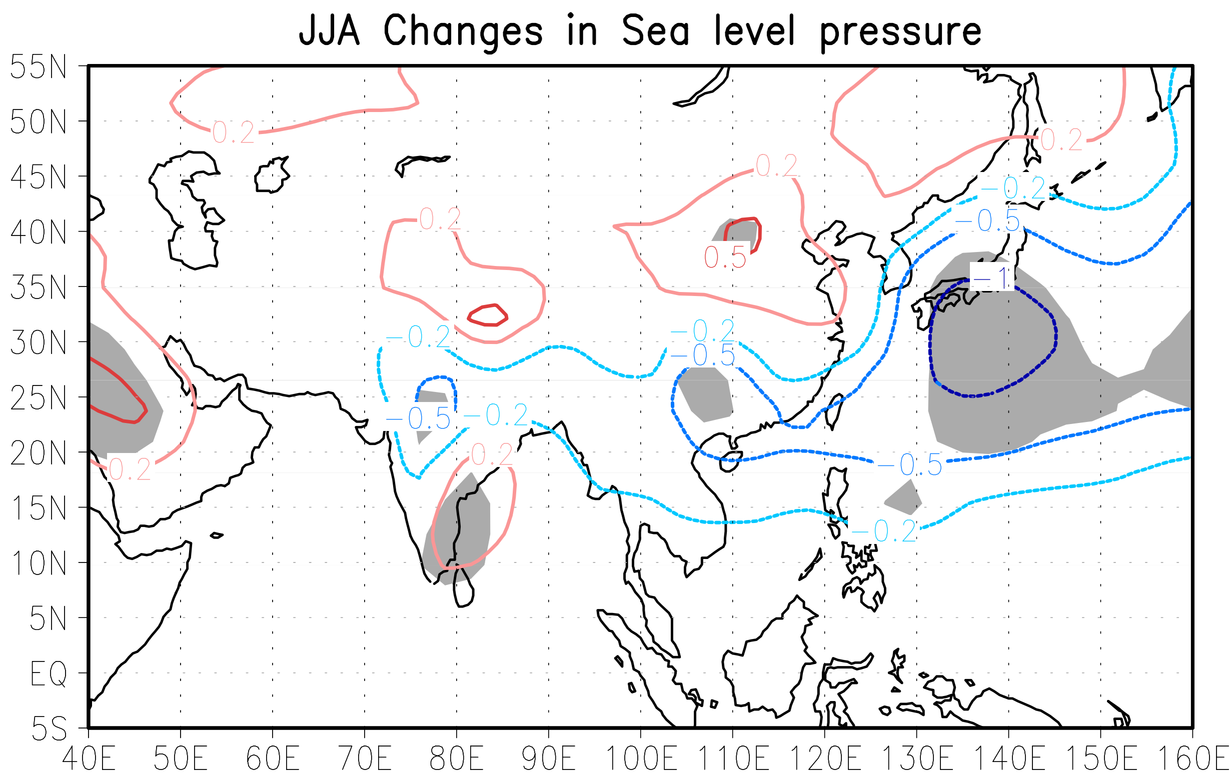

Fig. S4. June–August mean changes in sea level pressure (hPa) between 1700 and 1850. Shaded regions represent those in which the differences are statistically significant at the 95% confidence level.

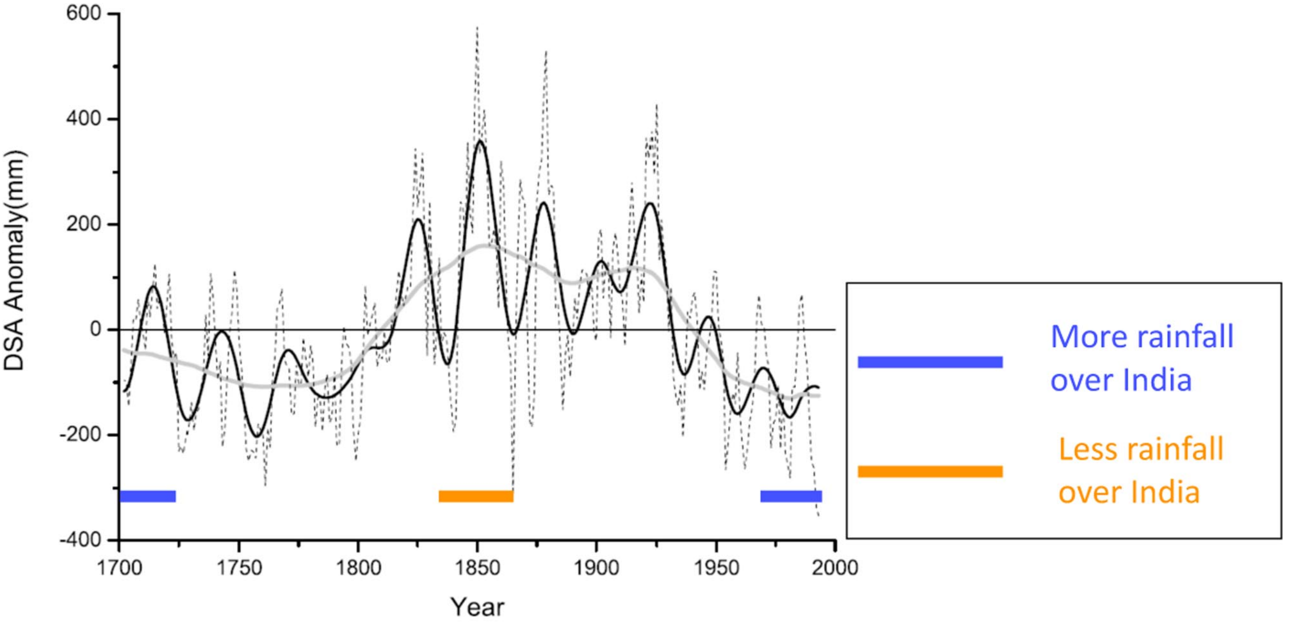

Fig. S5. Dasuopu snow accumulation (DSA) in Tibet–Himalaya and monsoon rainfall trends in Peninsula India (MRI). Three-year running mean of the DSA is shown by the dotted line, the reconstructed secular trend by the gray line, and the 26-year oscillation + trend by the solid line. MRI is negatively correlated with DSA (horizontal bars in lower part of the image) at a correlation coefficient of approximately −0.5. After figure 4 of Duan K, Yao T, Thompson LG (August 25, 2004) Low-frequency of southern Asian monsoon variability using a 295-year record from the Dasuopu ice core in the central Himalayas. *Geophys Res Lett*, 10.1029/2004GL020015, modified by permission of the American Geophysical Union.